European Polymer Journal 97 (2017) 169–177

Contents lists available at ScienceDirect

European Polymer Journal

journal homepage: www.elsevier.com/locate/europolj

Ionomer solution to film solidification dependence upon solvent type and its impact upon morphology and ion transport

Donghui Wang[a], YanFang Fan[b], Mingqiang Zhang[c], Robert B. Moore[c], Chris J. Cornelius[d,*]

[a] Envonik, Birmingham, AL 68588, USA
[b] College of Chemical Engineering, China University of Petroleum, Beijing, Changping District, 102249, China
[c] Department of Chemistry, Virginia Tech, Blacksburg, VA 24061, USA
[d] Department of Chemical & Biomolecular Engineering, University of Nebraska, Lincoln, NE 68588, USA

ARTICLE INFO

Keywords:
Ionomer
Morphology
Film solution-casting method and processing temperature
SAXS
FTIR
Proton conductivity

ABSTRACT

Ionomer chain and solvent molecule interactions during solution-casting, solvent evaporation, and solidification impacts chain entanglements, spatial arrangement of functional groups, microstructure development, morphology, and physical properties. These concepts were investigated using poly(*t*-butylstyrene-*b*-ethylene-*alt*-propylene-*b*-sulfonatedstyrene-*b*-ethylene-*alt*-propylene-*b*-*t*-butylstyrene) with a fixed ion-exchange capacity of 1.0, and estimated solubility parameter of 21.8 $(J/cm^3)^{1/2}$. Films were solution-cast using an equal volume cyclohexane:heptane mixture (C:H), chloroform ($CHCl_3$), and tetrahydrofuran (THF). Subsequent film structures were evaluated using transmission electron microscopy (TEM), small-angle X-ray scattering (SAXS), FT-IR, and electrochemical impedance spectroscopy. A commercially supplied film had sulfonated domains randomly distributed throughout it, and its initial proton conductivity was 11.8 mS/cm. A film created by solution-casting from C:H had a morphology containing randomly distributed sulfonated domains. This random morphology became more ordered with a lamella-like morphology when solution-cast using THF. The film produced from $CHCl_3$ had a morphology that was between random and ordered. Film morphology differences were attributed to a poorer solvent system that inhibited chain solvation. The solution-cast film's proton conductivity was 1.0 mS/cm for a random morphology, and 15.3 mS/cm with a lamella-like structure. Increasing the ionomer-THF solution-casting temperature to 40 °C produced a film with a 103% increase in conductivity (31.2 mS/cm). This led to a water uptake change from 29 wt% to 80 wt%. Cycling a THF solution-cast film from its dry to a wet state revealed that a lamella-like morphology would maintain its conductivity, but the commercial film's conductivity decreased from 11.8 mS/cm to 0.98 mS/cm. Ionomer film properties were found to be dependent upon solvent quality and processing.

1. Introduction

Ionomers are used as separation membranes in diverse fields such as electrodialysis, electrolysis, diffusion-dialysis, batteries, sensing materials, biomedical, analytical chemistry, and proton exchange membrane (PEM) fuel cells [1]. An ionomer has fixed charge carriers that are ionizable within an electrically neutral structure. This hydrophilic material transports ions [1–3]. Researchers have been synthesizing new ionomers in order to improve their physical properties for more than 60 years [3–7]. These efforts have focused upon optimizing composition and structure to maximize its morphology, physical and transport properties, thermochemical stability, and degradation resistance.

Ionomer properties are dependent upon the chain's spatial arrangement, which may give rise to lamellar, cylindrical, or a spherical morphology [8]. Zhao [9] and Lee [10] showed that sulfonated poly (ether ether ketone) (SPEEK) and poly(arylene ether sulfone)-b-polyimide copolymer ionomers containing longer hydrophilic domains triggered phase separation, which led to improved ion conductive domain organization. The resultant morphology had a remarkable increase in proton conductivity as compared to random copolymers. In addition to composition, processing methodology is incredibly important to properties. Solvent-type and casting temperature of SPEEK [11] and Nafion [5] led to large discrepancies in proton conductivity and chemical stability. Bebin and Galiano [12,13] demonstrated that solution-cast sulfonated polysulfone (sPSU) films had twice the proton conductivity as compared to melt-extruded sPSU. Weiss et al. showed that ion aggregate dissociation occurred at lower temperatures for block copolymers poly(*b*-styrene-*b*-(r-ethylene-so-r-butylene)-*b*-styrene)

* Corresponding author.
E-mail address: ccornelius2@unl.edu (C.J. Cornelius).

http://dx.doi.org/10.1016/j.eurpolymj.2017.10.011
Received 11 July 2017; Received in revised form 8 October 2017; Accepted 9 October 2017
Available online 10 October 2017

in comparison to similar homopolymers, which was attributed to microstructure [14]. Solution-casting and block length effects related to morphology, physical properties, and proton conductivity were studied using disulfonated poly(arlene ether sulfone) (BPSH-BPS) multi-block copolymers by Lee et al. [15]. This work revealed that BPSH and BPS block sizes of 5k:5k, 10k:10k, and 15k:15k led to a lamella-like morphology. In this study, the largest proton conductivity and lowest water uptake at any given ion-exchange capacity (IEC) was always improved with a multi-block ionomer versus a random one. Fan and Cornelius [16] explored the viscoelastic and gas transport properties of this BPSH-BPS multi-block copolymer as a function of block length (5k:5k, 10k:10k, and 15k:15k). Its thermally induced relaxation time dependence, and gas transport properties were evaluated. The efforts showed that smaller block lengths inhibited chain reptation and improved gas selectivity.

Choi et al. revealed that dilute poly(*t*-butylstyrene-*b*-ethylene-*alt*-propylene-*b*-sulfonatedstyrene-*b*-ethylene-*alt*-propylene-*b*-*t*-butyl styrene) solutions in cyclohexane:heptane (C:H) produced a spherical micellar morphology observed using X-ray scattering at an IEC of 1.0 and 2.0 [18]. These micelles had sulfonated styrene (sS) segments at its core, and the exterior chains primarily interacted with the solvent. This ionomer confirmation was adopted in order to lower its free energy to produce a more thermodynamically stable solution. Solution-casting this pentablock copolymer (PBC) into a film led to a morphology that contained sulfonated spherical micelles. These domains had a diameter ranging between 30 nm and 50 nm. Solution-cast PBC film morphology was studied based upon its degree of sulfonation (DS) at 26 mol% and 52 mol% by Mineart et al. [37]. Films solution-cast from THF had an ordered morphology that appeared to be composed of cylinders and lamellae. Wen and Cornelius demonstrated that solution-cast PBC with a DS of 31.2 mol% had a film morphology that transitioned from random to ordered using C:H and THF mixtures [31]. This ordered film morphology was a mixture of cylinders and lamellae when solution-cast from THF [31]. Increased morphological order within a film led to an improvement in modulus and proton conductivity. PBC films were converted into an ionomeric polymer-metal composite (IPMC), and its actuation performance was demonstrated to be morphology dependent. An IPMC using a film with a random morphology had a small actuation displacement and slow bending speeds. However, the PBC film having greater morphological ordered enabled rapid and large bending motions.

In this study, PBC with an IEC of 1.0 was solution-cast into films using THF, $CHCl_3$, and an equal volume C:H solution. These films were compared to commercially supplied films. Solution-cast film morphology and properties were studied using TEM, SAXS, and electrochemical impedance spectroscopy (EIS).

2. Experiment

2.1. Materials

Commercial PBC ionomer films (c-PBC) and solutions were provided by Kraton Polymers LLC, Houston, TX. This poly(*t*-butylstyrene-*b*-ethylene-*alt*-propylene-*b*-sulfonated styrene-*b*-ethylene-*alt*-propylene-*b*-*t*-butylstyrene) is synthesized using anionic polymerization. This PBC ionomer's block segments are abbreviated as tBS-EP-sS-EP-tBS for *t*-butylstyrene (tBS), ethylene-*alt*-propylene (EP), and sulfonated styrene (sS). The PBC chemical structure is shown in Fig. 1 [17]. After polymerization, the styrene block is selectively sulfonated to a desired IEC that represents milliequivalents of sulfonic acid per gram of polymer (mequiv/g). The degree of sulfonation (DS) is based upon the mole fraction of polystyrene PS, and sulfonated sPS blocks. The DS is the mole fraction of styrene blocks (S) that are sulfonated into sS. The complete PBC synthetic details have been documented elsewhere [17]. The IEC was equal to 1.0 for all PBC samples used in this study, and these materials are referred to as PBC1.0. Unsulfonated PBC is designed with a number average molecular weight of 78,000 g/mol and a polydispersity index (PDI) of 1.04. The unsulfonated molecular weights of tBS-EP-S-EP-tBS blocks are 15–10–28–10–15 kDa [31,30]. These properties are summarized in Table 1.

Table 1
PBC ionomer properties with different IEC [18,30].

	IEC mequiv/g	DS mol%	Density g/cm^3	tBS-EP-[S:sS]-EP-tBS kg/mol	Mass Ratio tBS-EP-[S:sS]
PBC0.0	0.0	0.0	0.958	15:10:28:10:15	0.385–0.256-[0.359:0.000]
PBC1.0	1.0	31.3	1.009	15:10:28.7:10:15	0.349–0.233-[0.207:0.211]

2.2. Film preparation

Commercial PBC films with an IEC = 1.0 (c-PBC1.0) were created from a C:H solution using a Doctor Blade "like" technique that was followed by rapid solvent evaporation [17]. c-PBC1.0 films were continuously prepared using a 50/50 vol% solution of cyclohexane and heptane (C:H). The process used a hot air oven with four heated zones operating between 38 °C and 98 °C with a film uptake speed between 9 and 21 m/min to generate films within minutes [17]. The process speed and conditions led to uniform and reproducible two mil films. Experimental PBC films were made form a dilute solution of either THF, $CHCl_3$, or C:H (1:1 vol%) containing 2.5 wt% ionomer. These solutions were solution-cast in a Teflon dish that was allowed to slowly evaporate to remove the solvent over a 36-h period at 25 °C. The evaporation space was a lab hood maintained at 30% Relative Humidity. All films were solution-cast at an elevation of 354 m or 97 kPa. The nominal thickness of each film was 60 μm.

2.3. Transmission electron microscopy (TEM)

A FEI Tecnai Biotwin G2 Spirit Transmission Microscope at 80 kV was used to acquire morphology images. All PBC samples were treated in a $BaCl_2$ solution to convert its acid-form to Barium-form in order to enhance its electron density contrast. This salt selectively exchanges with the SO_3H groups within PBC. Membrane strips with 0.5–1.0 mm width and 5.0–10.0 mm length were embedded in epoxy. Testing sections were cut using a Diatome diamond knife, and collected onto 400 mesh Copper Ruthenium grids.

2.4. Small angle X-ray scattering (SAXS)

Small-angle X-ray scattering was gathered using a Rigaku Ultima IV. The SAX instrument had a CuKα source and operated at 60 kV and 20 mA. The beam was collimated to a wavelength (λ) of 0.154 Å. Solution-cast films were evaluated by adjusting the incident beam angle θ from 0.03° to 1.76° using a 0.005° step size. This covered the total momentum transfer vector (q) from 0.0042 Å^{-1} to 0.25 Å^{-1}. This

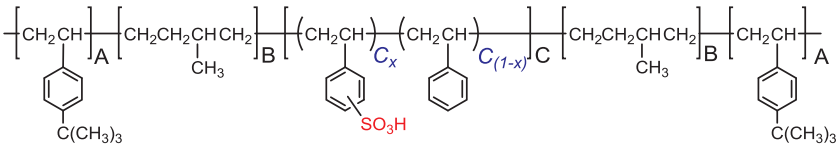

Fig. 1. Poly(*t*-butylstyrene-*b*-ethylene-*alt*-propylene-*b*-sulfonated-styrene-*b*-ethylene-*alt*-propylene-*b*-*t*-butylstyrene) structure.

relationship is given by Eq. (1).

$$q \equiv 4\pi/\lambda \sin[\theta/2] \quad (1)$$

2.5. Fourier transform infrared spectroscopy (FTIR)

FTIR was collected with a Nicolet *iS*10 spectrophotometer with a wavenumber resolution of 4 cm^{-1}. A spectrum was conducted in the attenuated total reflectance (ATR) mode with a single bounce ZnSe crystal using a scan rate of 16. The entire instrument was continuously purged with dry air during data collection.

2.6. Conductivity measurements

Nyquist impedance plots of fully hydrated PBC films were collected using a Metrohm Autolab PGSTAT302N from 0.1 Hz to 1 MHz. A two-probe method was used to measure its resistance (R) in the plane of the film with a BekkTech LLC test cell. The film's bulk R was obtained from a Nyquist impedance plot by interpolating the high-frequency arc to the x-axis. The distance between Pt electrodes was $L = 0.5$ cm, and the film's cross-sectional area was S. Test temperature was controlled using an isothermal water bath (Thermo Scientific Inc.). Film thickness was measured in its swollen state prior to an impedance test. Fully hydrated ionomer film conditions were created by submerging a film and allowing it to equilibrate in deionized water. The following equation is used to calculate a material's proton conductivity:

$$\sigma = L/(R \times S) \quad (2)$$

2.7. Film water uptake

Rectangular PBI films were used to determine water uptake. Prior to testing, dry films were soaked in deionized (DI) water at room temperature for 3 days to achieve equilibrium. The film's dry mass W_{dry} was measured after drying in a vacuum oven for 24 h. The fully hydrated films wet mass W_{wet} was quickly determined after dabbing excess surface water off it using as Kimwipe. The dry and wet film mass was measured gravimetrically, and its water uptake (WU) was evaluated using Eq. (3).

$$WU = 100*(W_{wet} - W_{dry})/(W_{dry}) \quad (3)$$

2.8. Estimated PBC and solvent δ and ε

PBC and solvent solubility parameters ($\boldsymbol{\delta}$) and dielectric constants ($\boldsymbol{\varepsilon}$) were calculated and compared to literature efforts. Fedor Data and group contribution methods (GCM) were utilized to estimate $\boldsymbol{\delta}$ values for PBC1.0, and its individual blocks [19]. These results are summarized in Table 2. The experimentally calculated EP, S, and sS blocks are $\boldsymbol{\delta_{EP}}$ = 16.9 $(J/cm^3)^{1/2}$, $\boldsymbol{\delta_S}$ = 21.9 $(J/cm^3)^{1/2}$, and $\boldsymbol{\delta_{sS}}$ = 31.4 $(J/cm^3)^{1/2}$. The $\boldsymbol{\delta_{EP}}$ result is in good agreement with previously reported EP elastomer $\boldsymbol{\delta}$ values ranging from 16.2 to 17.4 $(J/cm^3)^{1/2}$ [22]. Robeson [20] predicted a $\boldsymbol{\delta}$ for polystyrene (PS) between 15.6 and 21.1 $(J/cm^3)^{1/2}$ that is consistent with the predicted δ_S. Lu and Weiss [21] reported a $\boldsymbol{\delta}$ ranging between 18.6 to 33.9 $(J/cm^3)^{1/2}$ for sulfonated polystyrene (sPS) that was a function of IEC. The experimentally predicted $\boldsymbol{\delta_{tBS}}$ was 19.4 $(J/cm^3)^{1/2}$. This is close to Small and Hoftyzer and Van Krevelen's method predicting a value of 18.9 $(J/cm^3)^{1/2}$ [19]. Unfortunately, the tBS block has no reported experimental $\boldsymbol{\delta}$ values. However, Small and Hoftyzer and Van Krevelen methods provide a good prediction of it. An approximate $\boldsymbol{\delta}$ prediction is $\delta \approx 7.0$ ϵ that was demonstrated by Darby et al. [23]. This approximation was validated by Van Krevelen [19]. The PBC blocks degree of polymerization is n_{tBS}, n_{EP}, n_{PS}, and n_{sPS} are shown in Table 2 [19]. The solvent's Hildebrand values for dispersion ($\boldsymbol{\delta_d}$), hydrogen-bonding ($\boldsymbol{\delta_h}$), and polar ($\boldsymbol{\delta_p}$) forces are summarized in Table 3.

Table 3
Basic solvent properties [19].

Solvent	δ $(J/cm^3)^{1/2}$	δ_d $(J/cm^3)^{1/2}$	δ_p $(J/cm^3)^{1/2}$	δ_h $(J/cm^3)^{1/2}$	ρ (g/ml)	Mw g/mol	V_s (cm^3/mol)	ε
THF	19.5	16.8	5.7	8.0	0.889	72.1	81.2	7.58
$CHCl_3$	18.8	17.6	3.1	5.7	1.483	119.4	79.7	4.81
C:H	15.9	15.9	0	0	0.729	85.2	127	1.97

2.9. Flory Huggins solution theory

Flory-Huggins Solution Theory [24,25] is used to describe The excess Gibbs Free Energy (ΔG_m) for mixing a polymer and solvent (Eq. (4)). It takes into account molecule size and assumes Regular Solution behavior to describe the excess entropy (ΔS_m) and enthalpy (ΔH_m) of mixing.

$$\Delta G_m = \Delta H_m - T\Delta S_m \quad (4)$$

ΔH_m describes this mixture using a solvent (ϕ_1) and polymer volume fractions (ϕ_2), chi parameter (χ_{12}), ideal gas constant (R), absolute temperature (T), and solvent molar volume (V_s) (Eq. (5)).

$$\Delta H_m = \phi_1\phi_2\chi_{12}RT \quad (5)$$

ΔS_m is represented by the number of solvent and polymer segments occupying a lattice space (r_1 and r_2) shown in Eq. (6). This expression is used to model the configurational entropy of mixing.

$$\Delta S_m = R(\phi_1/r_1 \ln\phi_1 + \phi_2/r_2 \ln\phi_2) \quad (6)$$

χ_{12} is proportional to the interaction energy between polymer–solvent that is dependent upon δ. The predicted χ_{12} value is summarized in Eq. (7).

$$\chi_{12} = Vs/RT(\delta_1 - \delta_2)^2 \quad (7)$$

Table 2
PBC solubility parameter, volume fractions, and dielectric constant.

Polymer	δ $(J/cm^3)^{1/2}$	n_{tBS}%	n_{EP}%	n_{PS}%	n_{sPS}%	ε
		δ_{tBS} 19.4 $(J/cm^3)^{1/2}$	δ_{EP} 16.9 $(J/cm^3)^{1/2}$	δ_{PS} 21.9 $(J/cm^3)^{1/2}$	δ_{sPS} 31.4 $(J/cm^3)^{1/2}$	
PBC0.0	19.8	0.300	0.280	0.420	0.000	2.80
PBC1.0	21.8	0.282	0.263	0.250	0.206	2.97

n_x% is the block degree of polymerization and $\delta = \left(\frac{\sum(n_X\% \times E_{coh})}{\sum(n_X\% \times V_X)}\right)^{\frac{1}{2}}$.

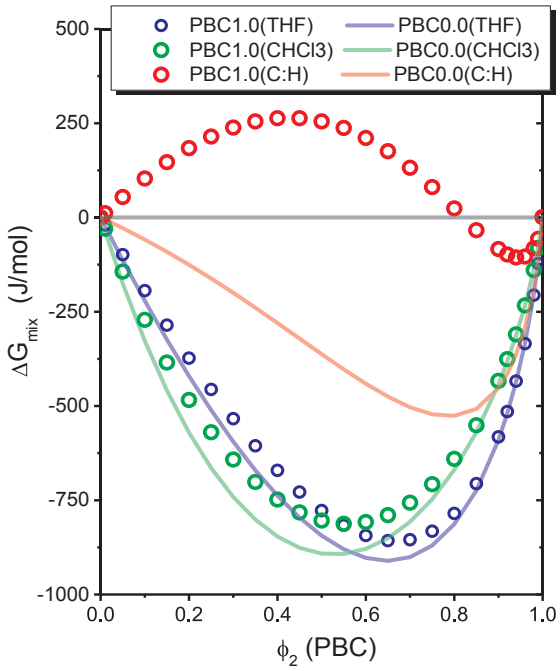

Fig. 2. Predicted ΔG_m solution behavior of PBC in C:H, $CHCl_3$, and THF.

3. Results and discussion

3.1. PBC1.0 solution to film predictions

The predicted χ values for PBC1.0 dissolved in THF, $CHCl_3$, and C:H are 0.095, 0.187, and 1.324. Unsulfonated PBC0.0 has χ values of 0.003, 0.032, and 0.717 for THF, $CHCl_3$, and C:H. A small χ becomes very important as the solvent evaporates during film formation. During this process, strong interactions cause ionomer chain aggregation and phase separation. This occurs in order to minimize the mixture's ΔG_m as it transitions from a dilute solution into a solid film during evaporation. The change in ΔG_m during this process was ideally modeled for PBC shown in Fig. 2.

PBC0.0 dissolved in C:H has a ΔG_m minimum (ΔG_m^*) equal to -310 J/mol at $\phi_2 = 0.80$. This value decreases to -910 J/mol using THF and $CHCl_3$ at $\phi_2 = 0.65$ and $\phi_2 = 0.55$. This thermodynamic result reveals that both THF and $CHCl_3$ are better solvents for PBC0.0 than C:H. Sulfonating PBC to create PBC1.0 leads to a positive ΔG_m^* when dissolved in C:H that indicates it is not a great solvent for this ionomer. This unfavorable solution (PBC1.0 and C:H) contributes to micelle formation that was previously observed by Choi et al. [18]. This C:H solvent behavior with PBC is attributed to it only having dispersion forces to solvate chains ($\boldsymbol{\delta_p} = \boldsymbol{\delta_h} = 0$). However, $\boldsymbol{\delta_p}$ and $\boldsymbol{\delta_h}$ are not zero for $CHCl_3$ and THF. $CHCl_3$ had $\boldsymbol{\delta_d}$, $\boldsymbol{\delta_p}$, and $\boldsymbol{\delta_h}$ values of 17.6 $(J/cm^3)^{1/2}$, 3.1 $(J/cm^3)^{1/2}$, and 5.7 $(J/cm^3)^{1/2}$; and THF had $\boldsymbol{\delta_d}$, $\boldsymbol{\delta_p}$, and $\boldsymbol{\delta_h}$ values 16.8 $(J/cm^3)^{1/2}$, 5.7 $(J/cm^3)^{1/2}$, and 8.0 $(J/cm^3)^{1/2}$. PBC1.0-THF and PBC1.0-$CHCl_3$ solutions had a ΔG_m^* of -860 J/mol and -810 J/mol at $\phi_2 = 0.65$ and $\phi_2 = 0.55$. Furthermore, ΔG_m is negative at all compositions suggesting a favorable ionomer-solvent system. These results imply that solution-casting films using THF and $CHCl_3$ may be excellent solvents for PBC because they are able to solvate chains better than a C:H. The sulfonate group within PBC1.0 affects its solvation characteristics due in part to hydrogen bonding. Interaction forces would facilitate tBS, EP, and sS solvation, which would minimize micelle formation, promote chain extension, increase chain entanglements, lower ΔG_m, and possibly improve ion-domain connectivity. These solvent-ionomer dynamics contribute to the formation of phase-separated structures during solution to film processing.

3.2. PBC film morphology

Ionomer solution to film processing is critical to its morphology and physical properties. A morphological study was investigated using PBC1.0. TEM and SAXS were done in order to evaluate solvent dependent microstructures. Solution-cast film morphology created from using C:H, $CHCl_3$, and THF was evaluated with TEM shown in Fig. 3. The unsulfonated blocks (tBS, EP, and S) are light domains, and sulfonated blocks (sS) appear darker due to preferential staining of sulfonate domains with electron-rich Barium. Fig. 3A reveals that sulfonated domains are randomly distributed within PBC1.0(CH) when C:H is used as a processing solvent. This morphology was observed by Fan and Cornelius et al. [26] as a function of IEC for PBC, which had WU and proton conductivity following Percolation Theory. PBC($CHCl_3$) films reveal a small increase in the relative spatial arrangement of sulfonated groups within PBC (Fig. 3B). Sulfonate domains appear to begin clustering into bundles of random intertwined tubes or sheets. Their relative spatial arrangement appears to increase in distance. This film morphology change suggests that sulfonated domains are being altered. These changes become pronounced with PBC films solution-cast from THF (Fig. 3C). These films reveal large-scale phase separation between sulfonated and unsulfonated domains. This morphology contains more continuous and wider spaced domains. Overall, ionomer film morphology progresses from random into lamellae-like or tube-like structures, which increase in size from $CHCl_3$ to THF. PBC1.0(C:H), PBC1.0($CHCl_3$), and PBC1.0(THF) solution-cast film morphology differences are related to solvent quality, and its ability to interact with PBC1.0. This result is associated with ΔG_m.

SAXS was used to examine morphology changes within the PBC1.0 films shown in Fig. 4A. All films had a maximum scattering peak (q_{max}) summarized in Table 4. If the first-order peak is assumed to be due to inter-domain interference, then Bragg's law ($d_{Bragg} = 2\pi/q_{max}$) can be used to estimate this distance between sulfonated domains [16]. The PBC1.0(C:H) solution-cast film had a strong primary scattering peak (q_{max}) at 0.201 nm^{-1}, and a very weak one at 0.401 nm^{-1}. The weak secondary peak suggests a relatively disordered microstructure. This scattering behavior is attributed to a more homogeneous distribution of ion-groups throughout the ionomer matrix, which is consistent with TEM data. PBC1.0(C:H) film's average inter-ionic-domain distance (IIDD) based upon q_{max} is of 31.3 nm. Utilizing $CHCl_3$ with a larger $\boldsymbol{\delta}$ to

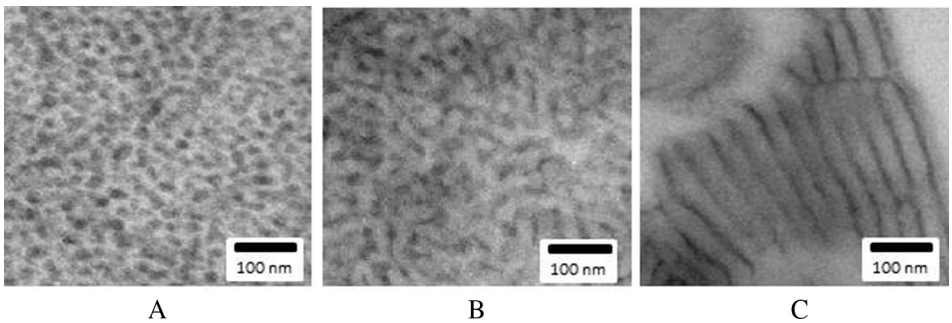

Fig. 3. PBC1.0(C:H), PBC1.0($CHCl_3$), and PBC1.0(THF) TEM images of solution-cast films at 20 °C using (A) C:H, (B) $CHCl_3$, and (C) THF.

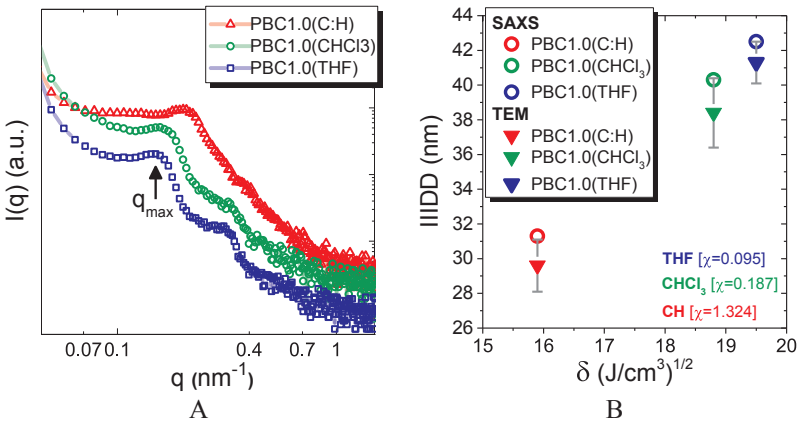

Fig. 4. (A) SAXS profiles of PBC1.0(C:H), PBC1.0($CHCl_3$), and PBC1.0(THF) films; and (B) average sulfonated domain IIDD estimates based on SAXS and TEM versus δ.

Table 4
PBC1.0 q_{max} and d-spacing in various solvent-cast films.

Solution-cast Film	q_{max} (nm^{-1})	$2q_{max}$ (nm^{-1})	$3q_{max}$ (nm^{-1})	d_1 (nm)
PBC1.0(THF)	0.148	0.321	0.532	42.5
PBC1.0($CHCl_3$)	0.156	0.327	0.554	40.3
PBC1.0(C:H)	0.201	0.401	–	31.3

solution-cast a PBC1.0($CHCl_3$) produced a film with three notable scattering peaks at 0.156, 0.327, and 0.554 nm^{-1} with an IDD increasing 28.8% to 40.3 nm. The multiple scattering peaks imply an increase in domain order that was noted in TEM (Fig. 3B). PBC1.0(THF) film's q shifted to a lower value with more discrete and intense scattering peaks at 0.148, 0.321, and 0.532 nm^{-1}, which had an average IIDD that increased 33.8% to 42.5 nm. PBC1.0(THF) maximum peak became stronger and sharper, which simultaneously shifted to a lower scattering value. This reveals that a greater distance exists between sulfonated domains. The solvent with a larger $\boldsymbol{\delta}$ (19.5 $(J/cm^3)^{1/2}$) and low $\boldsymbol{\chi}$ (0.095) produced a PBC1.0(THF) film with a more ordered morphology than films created using C:H and $CHCl_3$. These changes were enhanced with improved interactions between polymer chains and solvent molecules, which is reflected by a lower $\boldsymbol{\Delta G_m}$ predicted in Fig. 2.

All PBC1.0 solution-cast films had multiple scattering peaks, which is typically associated with a lamella-like morphology. A well-ordered lamellar morphology will have multiples of q_{max} [27]. However, PBC1.0 had approximate multiples of q_{max} that deviates at higher-order scattering peaks ($3q_{max}$). This result strongly suggests that these materials do not have a purely lamellar morphology, and it is most likely more complex. This is clearly observed using TEM, which revealed increased sulfonated domain order for PBC1.0($CHCl_3$) and PBC1.0(THF) films. The TEM and SAXS revealed that sulfonated domains tend to expand with increasing $\boldsymbol{\delta}$ and decreasing $\boldsymbol{\chi}$ used to create a solution-cast film. Greater solution $\boldsymbol{\delta_p}$ and $\boldsymbol{\delta_h}$ improves hydrogen bonding associated with the ionomer that also led to favorable interactions between tBS, EP, and sS blocks and chains. The ΔH_m improved from CH to THF as predicted by Eq. (5) with decreasing $\boldsymbol{\chi}$ (1.324 versus 0.095). This facilitated the development of a more ordered morphology as it transitioned from as solution to a solid film, which is attributed to a lower free energy state. A comparison between the global IIDD estimated using SAXS and TEM are shown in Fig. 4B. These independent techniques statistically agree with each other, and show that sulfonated domains within a film tend to expand with increasing $\boldsymbol{\delta}$ and decreasing $\boldsymbol{\chi}$.

3.3. Film processing dependent FTIR

FTIR spectra were used to identify and characterize PBC1.0 functional groups, and possible film changes due to solvent-casting at 25 °C. The PBC1.0(C:H), PBC1.0($CHCl_3$), and PBC1.0(THF) spectra are shown in Fig. 5. The FTIR absorbance was normalized using the phenyl group vibrational modes occurring from 1300 cm^{-1} to 1600 cm^{-1} wave numbers [28]. The $-SO_3H$ and $-SO_3^-$ groups appeared between 1000–1200 cm^{-1} with S=O asymmetric stretching noted at 1200 cm^{-1}, and symmetric modes visible at 1033 and 1005 cm^{-1}. The S–O vibration occurring at 1154 and 1125 cm^{-1} that has been noted in previous efforts [29,30]. However, weak aromatic ring vibrations occurring at 1100–1250 cm^{-1} overlapped with S=O asymmetric stretching and S–O vibrations. This led to poorer –SO_3H group distinction as compared with sharp and clear S=O symmetric stretching peaks. Significant film morphology changes were noted using TEM and SAXS, but it did not significantly influence the functional group

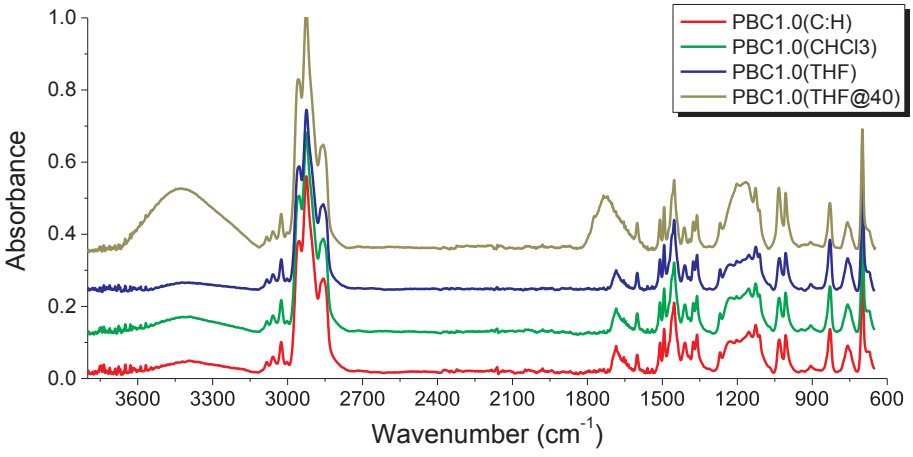

Fig. 5. FTIR of PBC1.0 solution-cast films as a function of solvent type and temperature.

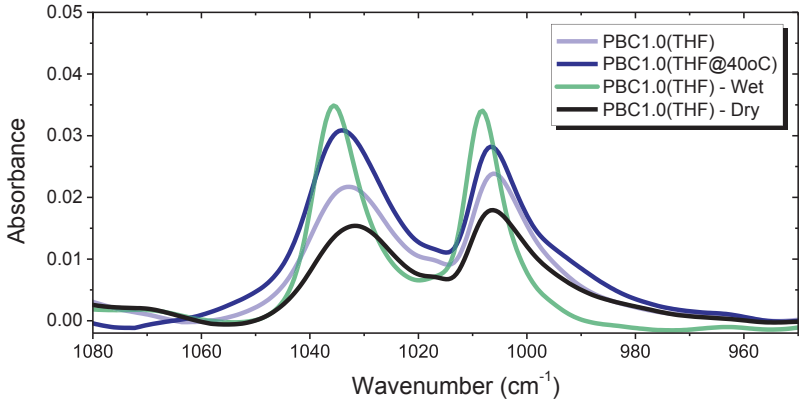

Fig. 6. FTIR of PBC1.0(THF) films wet, dry, and solution-cast at 20 °C and 40 °C between 1080 cm^{-1} and 950 cm^{-1} wavenumbers.

environment. However, at higher wave numbers, the characteristic −OH peak due to residual water and the $-SO_3H$ group water, which is noted between 3200 and 3600 cm^{-1}. In this region, PBC1.0(THF) films had a greater absorbance intensity that suggests more water bound to $-SO_3H$. A PBC1.0(THF@40 °C) solution-cast film at 40 °C from THF had the largest intensity change in this region than any film. This is attributed to greater clustering among sulfonated groups that accommodates more water within it due to morphology.

A film processing method that improves polymer solubility is solution-casting at an elevated temperature. This process impacts functional group spatial-arrangement within a film. Increasing the solution-casting temperature to 40 °C provides an additional 166 J/mol ($E = R\Delta T$) of energy that reduces hydrogen bonding between SO_3H groups and chains. This energy would enable ionomer chains to become more flexible, and partially overcome tBS, EP, S, and sS ($-SO_3H$) forces associated with ΔG_m. This produced films with greater functional group rearrangement noted in TEM and SAXS. The S=O asymmetric and symmetric, and S−O vibrational modes were clearly intensified due to the improved solvation and rearrangement of chains during solution-casting at 40 °C versus 20 °C. These changes are notable between 3200 and 3600 cm^{-1}, and the S=O symmetric stretching peak between 1031 and 1035 cm^{-1} that is associated with −OH and $-SO_3H$ peaks shown in Fig. 5. The enhanced absorbance is attributed to greater group clustering based on tBS, EP, and sS segments.

A PBC1.0(THF)-Dried film was created by putting it in a vacuum oven at 40 °C followed by an immediate measurement. This film had the smallest S=O stretching peak at 1031 and 1006 cm^{-1} shown in Fig. 6. This was compared to a PBC1.0(THF)-Wet film produced by soaking it in DI water, and immediately measuring it with excess water. The S=O symmetric stretching peaks became more intense within it, and shifted to 1035 and 1008 cm^{-1}. This corresponds to a 4 and 2 cm^{-1} wavenumber shift ($\Delta\nu$), which is attributed to hydrogen bonding. These molecular energy changes (ΔE) are described by $\Delta E = N_A hc\Delta\nu$ where h is Planck's constant, c is the light speed, N_A is Avogadro constant, and $\Delta\nu$ is the change in wavenumber [33]. These wavenumber shifts correspond to an ΔE of 23.9 J/mol and 47.9 J/mol that is attributed to a larger fraction of water interacting with sulfonated groups. PBC1.0(THF) and PBC1.0(THF@40 °C) films equilibrated at 30% RH had two sharp S=O symmetric stretching peaks at 1034 to 1007 cm^{-1}. The S=O symmetric stretching peaks remained at approximately the same wavenumbers. However, the PBC(THF@40 °C) film's intensity was 19% greater than PBC1.0(THF). The S=O intensity increase is associated with a greater SO_3H group concentration able to hydrogen-bond with water. Increased hydrogen bonding leads to greater interactions [28]. The S=O vibrational characteristic of RSO_2-OH complexed with water weakens its bond strength. This causes a wavenumber shift with increasing water concentration, which is notable in PBC1.0(THF) Dry and Wet films.

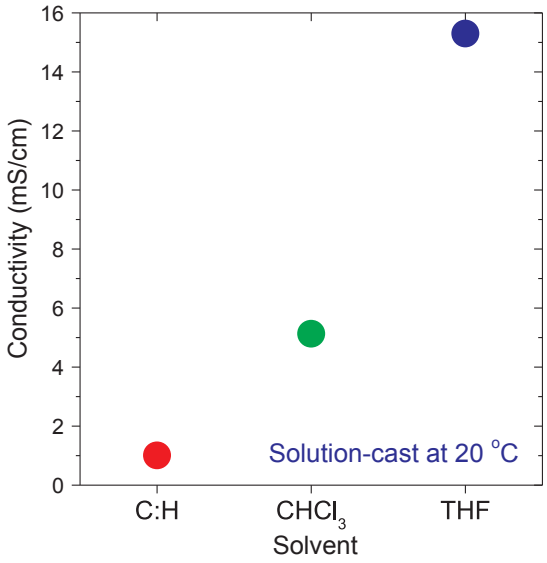

Fig. 7. PBC1.0 solution-cast film proton conductivity versus solvent-type.

3.4. Film processing dependent conductivity and percolation behavior

PBC1.0 proton transport differences are considered to arise from the solvent used to solution-cast a film, its ability to solvate chains, and processing conditions. As previously noted, ionomer films were solution-cast from C:H, $CHCl_3$, and THF, which led to an increasingly ordered morphology observed by TEM and SAXS. PBC1.0 proton conductivity changed with solvent $\boldsymbol{\delta}$ used to solution-cast a film in the following order: 1.01 mS/cm (C:H) < 5.13 mS/cm ($CHCl_3$) < 15.3 mS/cm (THF) that is shown in Fig. 7. Proton transport enhancements appear to be attributed to a lamellar-like morphology being created that increases from $CHCl_3$ to THF solution-cast films. The PBC1.0($CHCl_3$) film's morphology was in-between PBC1.0(C:H) and PBC1.0(THF). This organization structure of sulfonated domains produced a conductivity that was 5.13 mS/cm. Ion-transport differences between PBC1.0(C:H), PBC1.0($CHCl_3$), and PBC1.0(THF) films are attributed to better sulfonate domain spatial arrangement and connectivity. Film morphology changes produced a 5× and 15× improvements in proton conductivity using $CHCl_3$ and THF to solution-cast a film. Improving PBC1.0 chain solvation enhances their expansion, which assists in their probability of achieving a lower energy state. This is accomplished by improved chain and domain assembly, and greater morphological order that impacts ion transport. These changes were characterized by a transition from randomly distributed sulfonated domains to an increasingly structured material.

The relationship between solvent used to solution-cast a PBC1.0 film, and its conductivity are clearly important processing factors

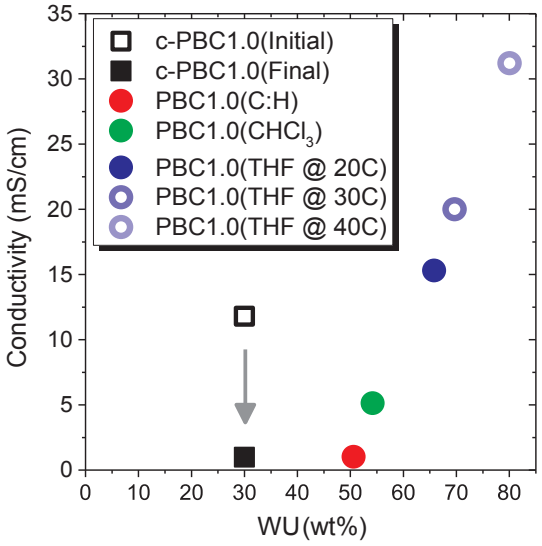

Fig. 8. PBC1.0 and c-PBC1.0 proton conductivity versus WU. PBC1.0(THF) conductivity is shown as a function of solution-casting temperature. c-PBC1.0 initial and final conductivity after cycling.

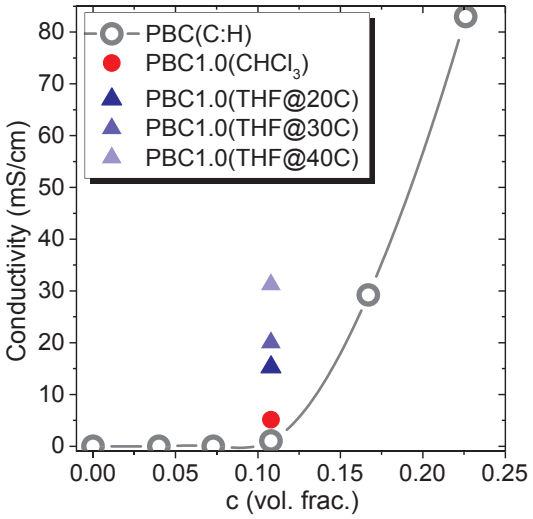

Fig. 9. PBC ionomer conductivity versus ***c***, and its relationship to PBC1.0(THF) films solution-cast at 20 °C, 30 °C, and 40 °C.

(Fig. 7). This was attributed to an improvement in chain solvation that contributes to a change from a random morphology into one with lamella-like structures. In this ionomer system, THF was the best solvent system for PBC1.0. However, there is a limit to its solvating ability that can be enhanced using thermal energy. PBC1.0 was solution-cast at 20 °C, 30 °C, and 40 °C using THF. This produced films with even larger proton conductivities that were associated with an equivalent rise in WU shown in Fig. 8. As previously noted, a PBC1.0(THF) film solution-cast using THF at 20 °C had a conductivity of 15.3 mS/cm. Solution-casting at 30 °C produced a film with a proton conductivity of 20.0 mS/cm, which increased to 31.2 mS/cm when solution-cast at 40 °C.

The commercial c-PBC1.0 film's initial proton conductivity was 11.8 mS/cm. This conductivity is greater than a solution-cast PBC1.0(C:H) film. As previous discussed, a c-PBC1.0 film is formed by a continuous solution-casting method with rapid solvent evaporation occurring within minutes using an elevated temperature ranging between 38 °C and 98 °C. This solution to solidification process does not provide sufficient time for PBC1.0 chains and blocks to adopt a lower energy state before becoming trapped as a solid. This rapid film-forming method and evaporation rate are very different from slowly solution-casting a thin film over 36 h. This elevated temperature produced a c-PBC1.0 film with a higher conductivity than PBC1.0(C:H). These differences are attributed to sulfonate group organization and connectivity.

Solution-casting temperature and solvent-type increased both conductivity and WU in a linear manner (Fig. 8). PBC1.0 film conductivity changes were directly proportional to WU, which increased from 50.6 wt% to 80.1 wt% for a PBC1.0(C:H) film versus PBC1.0(THF@40 °C). PBC1.0(THF) film's increased WU is attributed to greater connectivity between sulfonated domains. This facilitates more water molecules and enhances proton transport due to sulfonate group clustering, which widens lamella domains. The final c-PBC1.0 film state had a proton conductivity was 0.98 mS/cm, which is statistically the same as the experimentally solution-cast PBC1.0(C:H) (0.98 mS/cm versus 1.01 mS/cm). This change did not alter its WU of 29 wt% that may be due to subtle sulfonated domain connectivity differences.

PBC1.0 film's WU and proton conductivity displayed percolation behavior observed in Fig. 8. Percolation theory has successfully described a material's apparent diffusion and conductivity behavior using conducting and non-conducting sites. These sites would be sulfonated and unsulfonated domains within PBC. A limiting conducting site volume fraction (c_o) corresponds to its percolation threshold. The conducting site volume fraction (c), apparent conduction (σ_o), and a universal constant that only depends on spatial dimensions (β) can be used to model ion transport using Eq. (8). This relationship is applicable to any percolation system that is independent of material composition, structure, statistical properties, and morphology [38].

$$\sigma = \sigma_o(c - c_o)^{\beta} \tag{8}$$

This model was used to fit commercial PBC film (c-PBC) conductivity data as a function of IEC (0.4, 0.7, 1.0, 1.5, and 2.0) by Fan [39]. The c-PBC films had a c_o = 0.099, σ_o = 2.59e3, and β = 1.67. These values are consistent with numerous ionomer modeling efforts [38]. c-PBC ionomer's conductivity revealed typical conductivity percolation behavior of other random ionomers. PBC1.0($CHCl_3$) conductivity appeared consistent with c-PBC. This response may be due to its underdeveloped morphology. However, all PBC1.0(THF) films had larger conductivities than predicted for c-PBC, which has a random morphology. The larger conductivities must be due to improved inter-domain connectivity that occurs at the same R-SO_3H group concentration (c = 0.099). However, this assumption requires further experimental efforts directed at film processing and its relationship to morphology and transport (see Fig. 9).

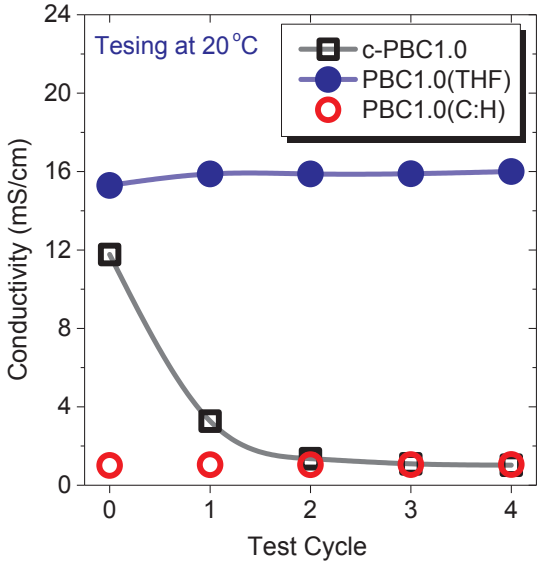

Fig. 10. c-PBC1.0, PBC1.0(THF), and PBC1.0(C:H) conductivity versus test cycle.

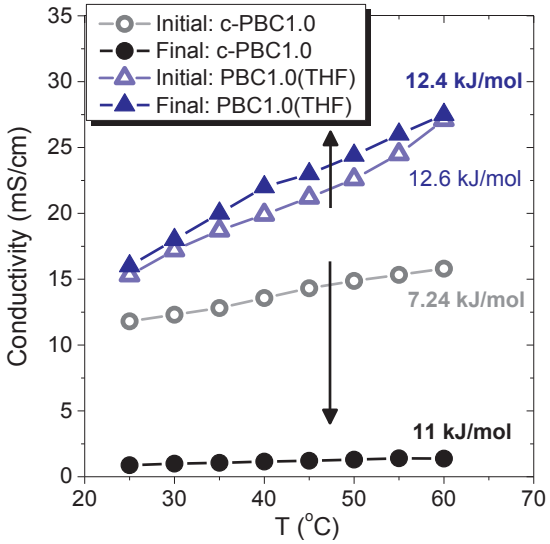

Fig. 11. PBC1.0(THF) and c-PBC1.0 initial and final temperature-dependent proton conductivity.

3.5. Film conductivity durability

An optimal solvent and casting temperature was shown to enhance morphology and transport. However, it may produce a film with poor stability due to excessive swelling, which is linked to phase-separation. c-PBC1.0 random morphology was previously shown by Zheng and Cornelius, and in this work [31]. The film's conductivity decreased after drying and rehydrating that was shown in Figs. 8 and 10. This conductivity decrease is striking because it appears to be related to the rapid film-forming technique used to create it. The fast c-PBC1.0 film processing method leads to a metastable structure due to insufficient time for polymer chain reptation to adopt a lower energy state. The film's decreasing conductivity is attributed to micro-structural fluctuations facilitated by the applied electric field (10 mV), cycling current, and water plasticized state. This facilitates block, chain, and sulfonate domain rearrangement needed to minimize the film's free energy. These changes decreased ion-domain connections that produced a dramatic decrease in proton conductivity from 11.8 mS/cm to 0.98 mS/cm. As previously noted, the solution-cast PBC1.0(C:H) film's conductivity is equivalent to the final c-PBC1.0 state. These results suggest that solution-cast films produce more stable proton conductivities. This is because polymer chains have greater time to achieve a lower energy state associated with functional group arrangement due to long solvent evaporation time. Solution-cast PBC1.0(THF) and PBC(C:H) films had small changes in proton conductivity after multiple test cycles (Fig. 10). In general, their conductivity slightly improved (~4%) after successive cycles, but remained constant with additional cycles. The stable PBC1.0(THF) film property is attributed to its lamellar morphology, which stabilizes ion domain connectivity that is associated with proton transport.

Proton conductivity is closely related with ion-cluster size, number, and spatial arrangement within an ionomer [36]. Improving the spatial order of sulfonated groups with a lamella-like versus a random morphology should impact film conductivity. These concepts were evaluated using pristine c-PBC1.0 and PBC1.0(THF) films. Their conductivity was evaluated from 25 °C to 60 °C using multiple cycles until its conductivity behavior reached steady-state (Fig. 11). Film conductivity stopped changing after four temperature ramping cycles. cPBC1.0 and PBC1.0(THF) film's initial and final temperature-dependent conductivity is shown in Fig. 11. c-PBC1.0 conductivity was initially 11.7 mS/cm that equilibrated to a final value of 0.88 mS/cm at 25 °C. This result is 10% lower than the rehydrating/hydrating cycles done at 25 °C (0.98 mS/cm). This additional decrease is associated with the additional thermal energy (60 °C) that increased chain motion needed to adopt a lower energy state. In contrast to this unstable behavior, PBC1.0(THF) film's conductivity changed from 15.3 mS/cm to 16 mS/cm. This very small change (~5%) reveals a stabilized property, which is attributed to its more ordered morphology.

c-PBC1.0 and PBC1.0(THF) films revealed a temperature-dependent conductivity that was Arrhenius [32–35]. This allowed its apparent activation energy (*Ea*) to be estimated. c-PBC1.0 film's *Ea* increased from 7.24 kJ/mol to 11 kJ/mol after thermal cycling. An *Ea* increase reveals that c-PBC1.0 has become more temperature dependent. This change is attributed to subtle sulfonated domain organization that requires additional studies. PBC1.0(THF) had an initial *Ea* of 12.6 kJ/mol that decreased to 12.4 kJ/mol after multiple cycles. This is considered not statistically significant. The relatively stable *Ea* is attributed to its morphology that stabilizes its transport characteristics. However, PBC1.0(THF) film's greater distance between sulfonated domains produced a higher *Ea* (12.4 kJ/mol), and temperature-dependent conductivity.

4. Conclusions

A relationship between PBC ionomer solution-casting and properties is linked to morphology and spatial arrangement of functional groups. An appropriate solvent (THF) altered its film morphology and proton transport at a constant IEC that was attributed to increasing δ and decreasing χ. Its morphology transitioned from a random distribution of sulfonated domains into an ordered material with micro-phase separation (lamella-like). PBC1.0(THF) films had an improved morphology over PBC1.0($CHCl_3$) and PBC1.0(C:H) as observed using TEM and SAXS. These changes were created using THF as a casting solvent that facilitated functional group rearrangement that produced films with better ion-transport properties. Film proton conductivity increased from 1.01 mS/cm to 31.2 mS/cm when solution-cast at 40 °C versus 25 °C. The lamella-like morphology of PBC1.0(THF) stabilized the film's conductivity when exposed to a continuous electric field and temperature cycling. However, the random morphology of c-PBC1.0 had a significant conductivity decrease that was attributed to this morphology and film processing technique. Previous ionomer film studies attempting to control morphology, physical properties, and transport characteristics have focused upon composition. This work provides a framework for ionomer improvements based upon solvent that is linked to ΔG_m.

Acknowledgements

This work was possible due to materials supplied by Dr. Carl Willis at Kraton Polymers LLC. Finally, we thank Mr. Stephen Daniels and the Bioscience Electron Microscopy Laboratory at the University of Connecticut for assistance with characterization studies.

References

[1] T. Sata, Ion exchange membrane, preparation, characterization, Modif. Appl. (2002) 1–307.
[2] A. Eisenberg, H.L. Yeager, Perfluorinated Ionomer Membranes, Wiley, New York, 1982.
[3] A. Eisenberg, J.-S. Kim, Introduction to Ionomers, Wiley, New York, 1998.
[4] D. Nguyen, C.E. Williams, A. Eisenberg, Block ionomer micelles in solution. 1. Characterization of ionic cores by small-angle X-ray scattering, Macromolecules 27 (1994) 5090–5093.
[5] R.F. Silva, M.D. Francesco, A. Pozio, Solution-cast Nafion® ionomer membranes: preparation and characterization, Electrochim. Acta 49 (2004) 3211–3219.
[6] C. Heitner-Wirguin, Recent advances in perfluorinated ionomer membranes: structure, properties and applications, J. Membr. Sci. 120 (1996) 1–33.
[7] K.D. Kreuer, On the development of proton conducting polymer membranes for hydrogen and methanol fuel cells, J. Membr. Sci. 185 (2001) 29–39.
[8] L.H. Sperling, Introduction to Physical Polymer Science (4th ed.). Bethlehem, PA: [3] John Wiley & Sons. ISBN Alger, Mark (1997). Polymer Science Dictionary (2nd ed.). London: Chapman & Hall. ISBN 0-412-60870-7. 2006.
[9] C. Zhao, H. Lin, K. Shao, X. Li, H. Ni, Z. Wang, H. Na, Block sulfonated poly(ether ether ketone)s (SPEEK) ionomers with high ion-exchange capacities for proton

exchange membranes, J. Power Sources 162 (2006) 1003–1009.
[10] H.-S. Lee, A.S. Badami, A. Roy, J.E. McGrath, Segmented sulfonated poly(arylene ether sulfone)-b-polyimide copolymers for proton exchange membrane fuel cells. I. Copolymer synthesis and fundamental properties, J. Polym. Sci. A 45 (2007) 4879–4890.
[11] G.P. Robertson, S.D. Mikhailenko, Casting solvent interactions with sulfonated poly (ether ether ketone) during proton exchange membrane fabrication, J. Membr. Sci. 219 (2003) 113–121.
[12] P. Bebin, H. Galiano, Processing of PEMFC membranes by extrusion: Part 1. Sulfonated polysulfone in acid form, Adv. Polym. Sci. 25 (2006) 121–126.
[13] P. Bebin, H. Galiano, Processing of sulfonated polysulfone for PEMFC membrane applications: Part 2. Polymer in salt form, Adv. Polym. Sci. 25 (2006) 127–133.
[14] X. Lu, W.P. Steckle, R.A. Weiss, Morphological studies of a triblock copolymer ionomer by small-angle x-ray scattering, Macromolecules 26 (1993) 6525–6530.
[15] M. Lee, R.B. Moore, J.E. McGrath, Effects of block length and solution-casting conditions on the final morphology and properties of disulfonated poly(arylene ether sulfone) multiblock copolymer films for proton exchange membranes, Polymer 50 (2009) 6129–6138.
[16] Y. Fan, M. Zhang, R.B. Moore, H.-S. Lee, J.E. McGrath, C.J. Cornelius, Viscoelastic and gas transport properties of a series of multiblock copolymer ionomers, Polymer 52 (2011) 3963–3969.
[17] C.L. Willis, Sulfonated block copolymers, method for making same, and various uses for such block copolymers. 2007.
[18] J.-H. Choi, A. Kota, K.I. Winey, Micellar morphology in sulfonated pentablock copolymer solutions, Ind. Eng. Chem. Res. 49 (2010) 12093–12097.
[19] D.W.V. Krevelen, P.J. Hoftyzer, Properties of Polymers, Their Estimation and Correlation with Chemical Structure, 1976.
[20] L.M. Robeson, Polymer Blend: a Comprehensive Review, Hanser Gardner Publications, Inc., 2007.
[21] X. Lu, R.A. Weiss, Development of miscible blends of bisphenol A polycarbonate and lightly sulfonated polystyrene ionomers from intrapolymer repulsive interactions, Macromolecules 29 (1996) 1216–1221.
[22] M.J. Forrest, Rubber Analysis: Polymers, Compounds and Products, iSmithers Rapra Publishing, 2001.
[23] J.R. Darby, N.W. Rouchette, K. Sears, Dielectric constants of plasticizers as predictors of compatibility with polyvinyl chloride, Polym. Eng. Sci. 7 (1967) 295–309.
[24] P.J. Flory, Thermodynamics of high polymer solutions, J. Chem. Phys. 9 (1941) 660–661.
[25] M.L. Huggins, Solutions of long chain compounds, J. Chem. Phys. 9 (1941) 440.
[26] Y. Fan, M. Zhang, R.B. Moore, C.J. Cornelius, Structure, physical properties, and molecule transport of gas, liquid, and ions within a pentablock copolymer, J. Membr. Sci. 464 (2014) 179–187.
[27] G. Gebel, Structural evolution of water swollen perfluorosulfonated ionomers from dry membrane to solution, Polymer 41 (2000) 5829–5838.
[28] M.R. Pereira, J. Yarwood, ATR-FTIR spectroscopic studies of the structure and permeability of sulfonated poly(ether sulfone) membranes. Part 1. —Interfacial water–polymer interactions, J. Chem. Soc., Faraday Trans. 92 (1996) 2731–2735.
[29] M. Ludvigsson, J. Lindgren, J. Tegenfeldt, FTIR study of water in cast Nafion films, Electrochim. Acta 45 (2000) 2267–2271.
[30] Y. Fan, C.J. Cornelius, Raman spectroscopic and gas transport study of a pentablock ionomer complexed with metal ions and its relationship to physical properties, J. Mater. Sci. 48 (3) (2013) 1153–1161.
[31] W. Zheng, C.J. Cornelius, Solvent tunable multi-block ionomer morphology and its relationship to modulus, water swelling, directionally dependent ion transport, and actuator performance, Polymer 103 (2016) 104–111.
[32] T. Thampan, S. Malhotra, H. Tang, R. Datta, Modeling of conductive transport in proton-exchange membranes for fuel cells, J. Electrochem. Soc. 147 (2000) 3242–3250.
[33] M. Saito, K. Hayamizu, T. Okada, Temperature dependence of ion and water transport in perfluorinated ionomer membranes for fuel cells, J. Phys. Chem. B 109 (2005) 3112–3119.
[34] C.H. Fujimoto, M.A. Hickner, C.J. Cornelius, D.A. Loy, Ionomeric poly(phenylene) prepared by diels-alder polymerization: synthesis and physical properties of a novel polyelectrolyte, Macromolecules 38 (12) (2005) 5010–5016.
[35] H. Hibbs, C.J. Cornelius, Ion transport in random and block sulfonated polyimides, J. Mater. Sci. 48 (3) (2013) 1303–1309.
[36] M. Saito, N. Arimura, K. Hayamizu, T. Okada, Mechanisms of ion and water transport in perfluorosulfonated ionomer membranes for fuel cells, J. Phys. Chem. B 108 (2004) 16064–16070.
[37] K.P. Mineart, X. Jiang, H. Jinnai, A. Takahara, R.J. Spontak, Morphological investigation of midblock- sulfonated block ionomers prepared from solvents differing in polarity, Macromol. Rapid Commun. 36 (5) (2015) 432–438.
[38] X. Tongwen, Y. Weihua, H. Binglin, Ionic conductivity threshold in sulfonated poly (phenylene oxide) matrices: a combination of three-phase model and percolation theory", Chem. Eng. Sci. 56 (2001) 5343–5350.
[39] Y. Fan, Structure, Physical Properties, and Transport of Multiblock Ionomers, Chemical Engineering, University Libraries University of Connecticut, Storrs, CT, 2012.